Multiple coated graphite oxide – sand composites for fluoride removal in water

Article *in* Journal of Environmental Chemical Engineering · January 2021

DOI: 10.1016/j.jece.2020.104962

10 authors, including:

W. P. R. T. Perera
University of Kelaniya
36 PUBLICATIONS **7** CITATIONS
SEE PROFILE

Jayani Bandara
National Institute of Fundamental Studies - Sri Lanka
2 PUBLICATIONS **0** CITATIONS
SEE PROFILE

Lakmal Jayarathna
National Institute of Fundamental Studies - Sri Lanka
30 PUBLICATIONS **158** CITATIONS
SEE PROFILE

Janitha A Liyanage
Department of Chemistry, University of Kelaniya, Sri Lanka
91 PUBLICATIONS **248** CITATIONS
SEE PROFILE

Journal of Environmental Chemical Engineering 9 (2021) 104962

Contents lists available at ScienceDirect

Journal of Environmental Chemical Engineering

journal homepage: www.elsevier.com/locate/jece

Multiple coated graphite oxide – sand composites for fluoride removal in water

A.R. Kumarasinghe [a,*], W.P.R.T. Perera [b], J. Bandara [c], P. Rukshagini [c], L. Jayarathe [c], Janitha A. Liyanage [b], R. Tennakone [d], A. Bandara [e], Xing CHEN [f], Rohan Weerasooriya [c,f,**]

[a] Department of Physics, Faculty of Applied Sciences, University of Sri Jayewardenepura, Nugegoda, Sri Lanka
[b] Department of Chemistry, Faculty of Science, University of Kelaniya, Sri Lanka
[c] National Centre for Water Quality Research, National Institute of Fundamental Studies, Kandy, Sri Lanka
[d] Faculty of Science and Technology, Uva Wellassa University, Badulla 90000, Sri Lanka
[e] Department of Chemistry University of Peradeniya, Sri Lanka
[f] Key Lab of Aerospace Structural Parts Forming Technology and Equipment of Anhui Province, Institute of Industry and Equipment Technology, Hefei University of Technology, Hefei 230009, PR China

ARTICLE INFO

Editor: Despo Kassinos

Keywords:
Graphite oxide
GO - sand composites
Water treatment
Sand filter
Fluoride

ABSTRACT

In drinking water treatment, sand filters are frequently used to remove turbidity. We enhanced the performance of the sand by a chemical modification using graphite oxide (GO). Repeated coating of sand granules with graphite oxide (GO) followed by low temperature (120 °C) pyrolysis yielded hierarchical core-shell structures. The sand granules can be coated with GO in a single (hereafter S-GO1) or multiple (presently five cycles, hereafter S-GO5) coating steps. The GO coated sand composites were characterized using spectroscopic, microscopic, and conventional techniques. When compared to S-GO1, the GO coatings on S-GO5 show enhanced stability in contact with water. The S-GO5 removes over 70% fluoride around pH 6.30 ± 0.02 according to Hill adsorption model. We also used a simulated water sample to assess the efficacy of sand/GO composites to remove fluoride and turbidity. When S-GO5 is used, the solution turbidity has reduced by 87% (from 0.08 to 0.01 NTU). However, in the presence of S-GO1, the turbidity has increased by + 75% (from 0.08 to 0.14 NTU). The gradual dissolution of adhered GO on S-GO1 enhanced the turbidity of treated water. The S-GO5 can be used to regulate excess fluoride and turbidity in water, simultaneously.

1. Introduction

Ingestion of high fluoride is harmful to human health. Approximately 60% of the human intake of fluoride originates from water consumption. The global prevalence of health implications due to the presence of high fluoride is not clear to date [1,2]. Elevated concentrations of fluoride in drinking water have caused tens of millions of dental and skeletal fluorosis cases worldwide over a range of years [1]. The systemic intake of fluoride in water may implicate neuro-toxicological effects, particularly during the early stages of human brain development [2]. Based on health risks for dental and skeletal fluorosis, the WHO guideline value for fluoride in drinking water is 1.5 mg/L. The WHO further recommends that individual countries should take into account water consumption and other sources of fluoride intake in setting up a standard for fluoride [3]. Therefore, the development of new methods for controlling fluoride at stringent levels in water is a pressing global priority.

To date, treatment methods based on reverse osmosis (RO), nano-filtration (NF), electro-dialysis self-reversal, precipitation-coagulation, and adsorption are used for water de-fluoridation [4 and references therein]. When compared to other methods, the treatment based on adsorption is widely used for water de-fluoridation due to its smooth operation and maintenance and low cost [5]. The commonly used de-fluoridation adsorbents include natural and processed mineral

* Corresponding author.
** Corresponding author at: National Centre for Water Quality Research, National Institute of Fundamental Studies, Kandy, Sri Lanka.
E-mail addresses: argk@sjp.ac.lk (A.R. Kumarasinghe), ruwantharangaperera@gmail.com (W.P.R.T. Perera), jayanibandara93@gmail.com (J. Bandara), ruks2007@gmail.com (P. Rukshagini), lakmalipj@yahoo.co.uk (L. Jayarathe), janitha@kln.ac.lk (J.A. Liyanage), sathyaruwini@gmail.com (R. Tennakone), athulatbandara@yahoo.com (A. Bandara), xingchen@hfut.edu.cn (X. CHEN), rohan.we@nifs.ac.lk (R. Weerasooriya).

https://doi.org/10.1016/j.jece.2020.104962
Received 30 May 2020; Received in revised form 9 December 2020; Accepted 16 December 2020
Available online 9 January 2021

oxides, tri-metal oxide composites, carbonaceous materials such as activated carbon, carbon nanotubes (CNT), graphene and graphene derived substrates [6,7]. When compared to other de-fluoridation adsorbents, only a few reports are available on the use of graphite oxide, or graphene as de-fluoridation adsorbent [6,7]. Graphene oxide characterizes with randomly distributed aromatic regions (sp^2 *C*) and oxygenated aliphatic regions (sp^3 *C*) containing surface hydroxyl, epoxy, carbonyl and edge carboxyl groups [8]. Graphene oxide readily aggregates in water and polar solvents through π-π interactions forming graphite oxide. Therefore, graphite oxide (GO) encompasses several layers of graphene oxide. Li et al. [7] showed over 80% removal of fluoride by graphene particulates at pH 7.00. Although graphene efficiently removes fluoride, the separation of fluoride-rich graphene particulates from the treated water poses an additional problem, and some cytotoxic effects of graphene are also reported [9]. When compared to graphene, GO did not cause any significant toxicity to cell growth and proliferation [10].

On the other hand, ordinary sand is the oldest water treatment material used to remove suspended solids, turbidity and microorganisms by granular filtration. The surface sites on natural sand are dominantly negative, i.e., $pH_{zpc} = 2.10$, and chemically inert [11]. Therefore, they show a low affinity for most of the contaminants dissolved in drinking water. We enhanced the performance of sand by applying multiple coated graphite oxide layers onto sand grains, hereafter referred to as reactivity enhanced sand. Sotirelis and Chrysikopoulos [12] have shown graphene oxide retention on quartz sand due to chemical interactions. However, the stability of graphene oxide layers on sand upon prolonged exposure to water is not examined in detail. Besides, GO layers were coated on sand using various chemical binders and chemical grafting methods. For example, Sutter et al. [13] grafted aromatic thiols on carbon domains in graphite oxide without using intermediates while preserving hydrophilicity. Gao et al. [14] grafted sand ≡SiOH groups with $–NH_2$ and GO attached to the sand surface via coupling agents. However, the use of binders introduces additional complications to the system, and the surface properties of sand may not be fully augmented as expected due to not having a direct linking between graphene and sand. Therefore, we proposed direct adhesion on sand using inherent properties of graphite-based substrates.

2. Materials and methods

2.1. Materials

Natural vein graphite (NVG) was collected from Sri Lanka (location: 7° 06' 58.49'', 80° 18′ 34' 41'' Sri Lanka). The ash content of NVG was above 99.95% [15]. The sand was collected from the Mahaweli River (Sri Lanka 8° 27' 59.99" N; 81° 13' 60.00" E, Sri Lanka). A turbidity standard (100 ± 2% NTU) was received from Thermo Scientific (USA). Other chemicals used are analytical grade as received from Sigma-Aldrich (USA), BDH (UK) or Fluke (Switzerland). Ultrapure water was used during the experiments.

2.2. GO - sand composites synthesis

The powdered NVG flakes were passed through ASTM no 40 sieve. The sieved NVG was used to synthesize graphite oxide (GO) by a modified Hummers method [15]. Fig. 1-S (support documentation) shows detailed steps of GO preparation by a modified Hummers method. The GO was washed with distilled water several times until the solution pH became neutral. The solid content of the GO - water slurry was determined, gravimetrically. An aliquot of GO water/slurry was diluted with distilled water to yield a suspension of 1.00 ± 0.01 g/L GO. The GO suspension was ultrasonicated for 30 min (150 W, Grant, UK) and was kept under stirring (e.g. 120 rpm) at room temperature for 24 h. An aliquot of the 1.00 (± 0.01) g/L GO suspension was placed on freshly cleaved mica surface for atomic force microscopy (AFM) imaging. We measured the average lateral dimension and thickness of exfoliated GO layers as ~ 2 μm and ~ 1 nm, respectively by AFM (NC-AFM, Park Systems XE 100, Korea).

The sand was fractionated according to grain size using stainless steel sieves (ASTM E11 no 40 (⌀ 0.420 mm) and no 30 (⌀ 0.600 mm)). The uniformity coefficient (C_u), the specific gravity, and the bulk density of the quartz sand were 1.24, 2.6 g/cm^3, and 1.6 g/cm^3, respectively. The specific surface area of sand used was determined as 70 cm^2/g (Quanta Chrome Instruments ver. 11.0, Anton Paar, Austria). To remove surface impurities (e.g. metal (hydr) oxides, and organic coatings), following cleaning cycle was used: i. soaked in ~ 0.1 M HNO_3 (~ 6.5 mL of 70% v/v HNO_3 in 1 L solution) for 3 h, ii. Rinse with distilled water to remove HNO_3 traces, iii. Soaked in ~ 0.1 M NaOH for 3 h, and iv. Rinse with distilled water to remove NaOH traces. The cleaned sand samples were dried at 110 °C in an oven for 2 h (PCH C6000, BIOBASE, China)., and stored in a dessicator. A 10 g of the dried sand was mixed with 10 mL 0.35% GO – water suspension around pH ~ 4.5, and the mixture was heated at 120 °C using an oven (PCH C6000, BIOBASE, China). Following the heating, the brownish colour sand turned into black, which indicates the coating of GO on sand. This process was repeated several times to adhere GO coating on the sand firmly. Hereafter, we used the following notation; S-GO1: GO coated on the sand in one cycle; S-GO5: GO coated on the sand in five cycles. The term S-GO denotes both S-GO1 and S-GO5 composites (Figure 6-S: Support documentation). To verify the existence of GO on the sand surface, we performed Raman spectroscopic measurements of graphite, GO, sand, S-GO1 and S-GO5 samples.

2.3. S-GO1 and S-GO5 characterization

The IR spectra of sand and GO - sand composites were recorded with an FTIR spectrometer supplied with a DLaTGS detector and ZnSe ATR cell (model iS50 and SMART iTR, Thermo Scientific, USA). All spectra were obtained at 4 cm^{-1} resolutions in the 400 – 4000 cm^{-1} spectral range (64 scans, gain 1, and attenuation 0). Raman spectra were also measured at 532 nm laser excitation with a confocal Raman microscope (LabRAM HR 800, Horiba Jobin Yvon, Japan). X-ray diffractograms of sand and sand-GO composites were obtained for phase identification. An X-ray diffractometer at 20 kV and 30 mA was operated using Cu-K_α radiation at λ = 0.154 nm (Rigaku Ultima IV, Japan). The morphology of the sand and S-GO composites was imaged by scanning electron microscopy (model Zeiss Quanta 650 FEG). The effects of carbon derived materials on EDX measurements in SEM are well known, and these effects were taken into consideration in the data presented.

The point of zero proton charges of S-GO1 and S-GO5 (e.g. pH_{pnzpc}) were determined by surface proton titrations using calibrated 0.095 M NaOH. The 5 M $NaNO_3$ was used to control the background ionic strength of the solution from 0.001 to 0.1 M. We used a flow-cell apparatus combined with auto titrator (model, KEM AT 610, Japan) to conduct protons titrations by varying pH from 4 to 9. The titration data were processed to obtain pH_{pnzpc} of S-GO1 and S-GO5 (support documentation Figure 6-S. A–B).

2.4. Fluoride adsorption isotherms

The fluoride adsorption isotherms were constructed for S-GO composites at pH 7.00 ± 0.02 and 0.01 M $NaNO_3$. Batches were prepared in triplicate at each condition. To each 50 mL capacity centrifuge tubes that contain 20 mL distilled water and 50 μL of 5 M $NaNO_3$, 0.0225 g of S-GO composites (S-GO1 or S-GO5) were added. The S-GO suspensions were equilibrated for 12 h on an end-or-end shaker (MS-RD-Pro Rotor, HINOTEK China). After that, predefined aliquots of 100 mg/L fluoride stock solutions were added into the tubes to reach initial fluoride concentration between 0.50 and 2.50 mg/L. After the pHs of the S-GO suspensions were adjusted with 0.120 M NaOH to 7.00 ± 0.02, and they were equilibrated for 5 h at 298 K. Several hours before completion of

the equilibration the pHs of the batches were readjusted if required. After the final pH values were recorded, they were centrifuged followed by filtration with 0.22 μm nylon membrane filters. The adsorbed amounts of fluoride were calculated by subtracting the dissolved F^- concentrations from the initial F^- concentrations.

2.4.1. Fluoride and turbidity removal by S-GO composites

The concurrent efficiency of fluoride and turbidity removal by 0.90 ± 0.01 g/L of S-GO composites was determined using a simulated water sample with the composition: pH 6.30 ± 0.01, 2 mg/L fluoride, and 0.08 ± 0.01 NTU turbidity. Similar to the batch experiments, four suspensions (two each from S-GO1 and S-GO5) were equilibrated at predefined periods. The fluoride and turbidity concentrations of the solution were measured within an hour. In a separate study, the batch mixtures with a similar composition were kept for two months. The efficiencies of fluoride and turbidity removal by S-GO composites were determined as follows:

$$Fluorideadsorptioncapacity \quad , \quad mg \Big/ g = \frac{[F^-]_{initial} - [F^-]_{final}, \quad mg \Big/ L}{[solidcontent], \quad g/L}$$

$$\% \quad Turbidityremoval \quad = \quad \frac{[turbidity]_{initial} - [turbidity]_{final}}{[turbidity]_{initial}} x \quad 100$$

2.4.2. OH^- / F^- exchange ratios

In all F^- adsorption, due to the exchange of OH^- for F^-, the pHs of the S-GO suspensions were increased. We measured the F^-/ OH^- exchange ratio ($r_{F/OH}$) of the simulated water and S-GO suspensions. Before solid and solution separation, the pH of the S-GO suspensions was adjusted to 6.30 ± 0.02 with pH-statted titrator (Metrohm 907 Titrando, Switzerland) using 0.125 M HNO_3 to estimate OH^-/ F^- stoichiometric exchange ratio upon fluoride adsorption as detailed in ref. [16].

2.5. Kinetics study

Chemical kinetics of fluoride adsorption on S-GO composites was conducted in a water-jacketed batch reactor. A 500 mL of 0.90 ± 0.01 g/L S-GO composites (S-GO1 or S-GO5) and 1.00 ± 0.01 mg/L fluoride solution was prepared in the reactor under continuous N_2 purging. The suspension pH was always regulated at 7.00 ± 0.02 by adding 0.125 M HNO_3. The suspension of S-GO composites (S-GO1 or S-GO5) was stirred continuously while 1 mL aliquots were withdrawn in triplicate (within < 1 min) at predefined time intervals and the solid and liquid were separated instantly and fluoride concentration of supernatants was measured.

2.6. Analytical methods

The solution F^- concentrations were measured either with a combined ion-selective electrode (ISE) (Model Orion 9609BNWP) or Metrohm 907 Titrando or non-suppressor ion chromatography (Shimadzu CBM-20A, Japan). Detection limits for ISE (0.005 mg/L) were better than non-suppressor ion chromatography for fluoride. Therefore, to detect fluoride below 1.00 mg/L, the ISE method was used. Spike recoveries of the 0.01 mg/L F^- the solution was 97% and 95% from IC and ISE measurements, respectively. The pH 4.00 ± 0.02, 7.00 ± 0.02, and 9.00 ± 0.02 buffers (Metrohm, Switzerland) were used in the pH electrode calibration. The multi-parameter analyzer was used to determine TDS/EC in the samples (HI 9811–5, Hanna USA, EC resolution 0.01 mS/cm). The turbidity measurements were also carried out of the same samples by a turbidity meter (EUTECH TN-100, Thermo, USA, resolution 0.01 NTU). The average of triplicate measurements resulted in the reported pH, turbidity, fluoride concentrations.

3. Results and discussion

3.1. Morphological and structural characterization

Graphite oxides (GO) have intercalated water, and its exfoliation yields graphene oxide single sheets with an edge -COOH, basal –OH, and structural epoxy groups. When these functional groups are removed from graphite, reduced graphene oxide is formed. According to AFM measurements, our GO has an average lateral dimension ~ 2 μm and thickness ~ 1 nm (Fig. 2-S). A cross-sectional FE SEM image of GO shows of multilayer structures (Fig.3-S). Therefore, the Hummers treatment of vein graphite results in graphite oxide (GO).

The SEM images and energy-dispersive X-ray (EDX) spectral data recorded from sand, graphite oxide (GO), and sand-graphene oxide composites are shown in Fig. 1.A–D and Fig. 5-S.A–D. River sand, typically used in drinking water treatment, shows the gradational distribution of euhedral sand grains with clustering (Fig.1.B). The surfaces of euhedral crystals are smooth without pits, grooves, and deformities (Fig. 1.B). The SEM micrograph shows GO layer disorder upon multiple coating on sand (Fig. 1.D). The chemical composition of river sand and different GO composites is summarized in Table 1.

Presumably, the peak for C may have originated from contaminants present on the sand. In vein graphite, minute proportions of Fe and silica are well-documented [15]. In GO, the prominent EDX peak for C originates from the basal plane carbon atoms (Fig. 5-S. A); Si and Cl occur in smaller concentrations when compared to sand. The C originates predominantly from precursor graphite in GO. The Cl, Si and S originate from the precursor graphite and the chemicals used for graphite → graphite oxide conversion. Both flake and needle-like structures found in natural vein graphite [15]. However, GO does not have any flaky or needle-like morphology, but graphite does. The openings present amidst GO sheets are tunable [17].

Fig. 1-C and D show the SEM images recorded from graphite oxide coated sand. The interface between GO and sand is evident that GO is present on the sand as an overlayer. A rugged morphology for the bare sand surface can be seen here (Fig. 1C, S-GO1). However, when analyzing many images taken under the same conditions, it came into light that the GO layer does not extend/spread on sand continuously but leaving behind some uncoated areas of sand (Fig. 1C). GO has chemisorbed onto defects-enriched sand surface sites due to the creation of a local environment leading to adsorption even under unfavourable conditions [18]. Nevertheless, when the number of GO coating is increased, the uncoated areas on sand particles gradually diminish, and the thickness of the GO layer on sand increases (Fig. 1D). Besides, the rough morphology observed for uncoated areas of sand (Fig. 1A) become even (smooth), indicating GO deposition.

To verify the existence of GO on the sand surface, we performed a Raman experiment, and the data are shown in Fig. 2. (a). The Raman peaks of 1350 cm^{-1} (D band) and 1590 cm^{-1} (G band) reveal the existence of GO (Fig. 2.a. B, D and E). And also, there are no obvious SiO_2 peaks (Fig. 2.a. C) in S-GO1 (Fig. 2.a. D) and S-GO5 (Fig. 2.a. E) within the region where the peaks for graphite and GO appears (Fig. 2.a. C spectrum for the sand); this might be attributed to the significant coverage of sand with GO. When sand granules are multiply coated, the GO layers seem hierarchical resulting GO/sand core shells as supported in SEM and EDX data. Last but not least, the change of colour of sand from white to black after the coating of GO is apparent even visually as shown in the as photo images (Fig. 2.b. C, D and E).

Furthermore, the laboratory XRD measurements were carried out to determine graphite → GO conversion and crystallinity of river sand. However, they (viz. XRD data) cannot use to identify GO coatings on the sand. The negation of XRD measurements in identifying GO coatings on the sand and the use of Raman data to resolve this ambiguity deserves a discussion. In the case of graphite (Fig. 4-S; support documentation), we observe the diffraction from (002) crystal plane at 26.7°. For sand, the (011) plane exists at 26.6^0 for quartz (river sand consists of quartz and

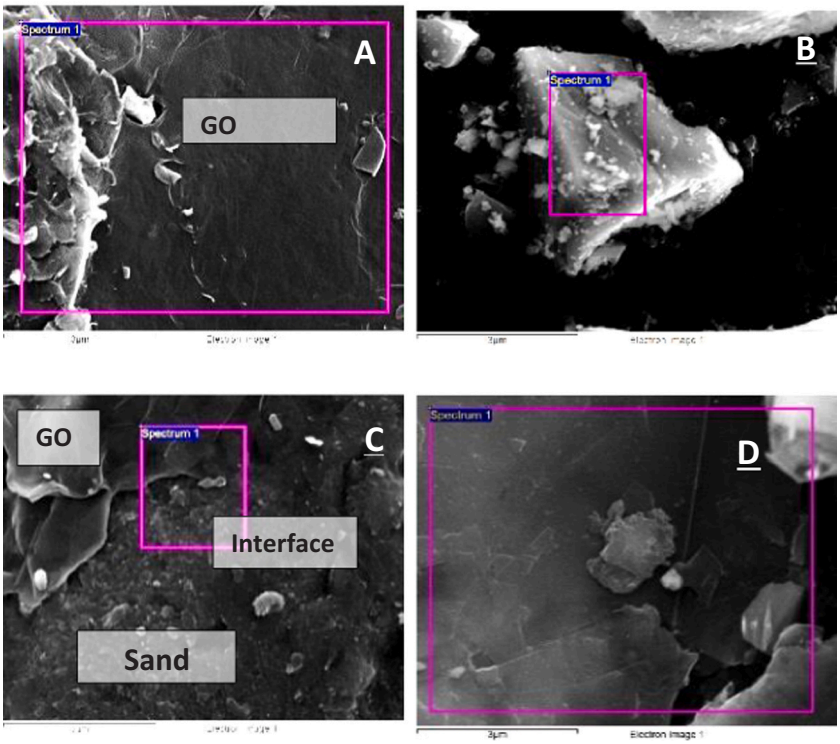

Fig. 1. (A-D): SE-SEM images of A. Graphite oxide (GO), B. River sand (S), C. Singly GO coated sand composite (S-GO1); D. Multiple GO coated sand composite (S-GO5).

Table 1
The elemental composition of river sand, graphite oxide, S-GO1 and S-GO5 (refer to Fig. 5-S:A-D for EDX details).

Material	Weight composition ± 1–12% RSD						
	C	O	Si	S	Al	Cl	Fe
River sand	17.70	60.81	21.37	–	0.13	–	–
Graphite oxide, GO	67.04	32.22	0.09	0.55	–	0.10	–
Sand + GO (S-GO1)	24.65	53.58	20.97	–	0.80		
Sand + GO (S-GO5)	95.43	4.38	0.11		–	–	0.14

mica). For GO, the (001) plane appears at 10.3°. The XRD peaks for sand (011) and graphite (002) lie very close to each other and practically indistinguishable. In graphite, the disappearance of the characteristic 2θ peak at 26.10°, and the appearance of the GO peak around 10.04° confirms the conversion of graphite → GO (Fig. 4-S. B). Graphite and sand peaks around 26° are very close to each other (Fig. 4-S. A and C). In singly GO coated-sand (S-GO1), the peak at 26.1° corresponds to sand is shown (Fig. 4-S. E). However, the characteristics peak of GO at 10.04° disappeared, possibly due to the disordered nature of GO upon the coating. In multiple GO coated- sand (S-GO5), characteristic peaks for neither GO nor sand peaks discern since sand granules seem to cover with disordered GO sheets (Fig. 4-S. D). In concurrence, the weight composition of Si in S-GO5 and S-GO1 is 0.12% and 20.97%, respectively (Fig. 5-S. C and D).

The GO peak at 10.04° disappeared both in S-GO1 and S-GO5, which indicates disordered GO layering. The sand peak at 26.2° diminished upon multiple GO coatings. Single layered graphene or graphene oxide sheets are featureless under XRD (2θ < 15°), and the XRD patterns of several layered GO is relatively weak than that of pure GO [19]. The formation of amorphous C layering on sand is unlikely at 120 °C. However, at this temperature, most of the intercalated water and oxygen-containing functional groups in the interlayers of graphite oxide are removed [20]. As the heating is progressing, in the presence of sand with a high degree of surface inhomogeneity and irregularity, graphite oxide could adhere in a fully exfoliated manner due to reduced interlayer interactions. Presumably, this reduction and exfoliation process might be taking place concomitantly with a competition, which to some extent explains for not having (or having slightly) a peak close to graphite peak in S-GO1 and S-GO5. The new exfoliated structures result in highly disordered GO on the sand with weak or no XRD signature. Finally, we are convinced that the ambiguity on the presence of GO on sand can resolve by using high-resolution XRD using synchrotron radiation.

3.2. Spectral characterization of surface interactions between S-GO composites and F

As shown in Fig. 3.I.A–E, the functional groups of GO, sand, and S-GO composites and their interactions with fluoride in water are characterized by Fourier Transform IR spectroscopy (the efficacy of S-GO composites in water defluorination is described in Section 3.3). The broad and intense band at 3420 cm^{-1} of GO corresponds to the stretching vibrations of –OH functional groups of physiosorbed H_2O (Fig. 3.I.A). In most environments, the –OH groups do not exist in isolation, and a high degree of association is experienced as a result of extensive hydrogen bonding with other hydroxyl groups. The –OH groups may be within the same plane, or they most likely exist between adjacent graphene layers. The extensive H-bonding results broadened the IR band with reduced mean absorption frequency. If –OH groups are in isolation, the absorbance bands are narrow and observe at high wavenumber [21]. As shown in Fig. 3.I.A, the shoulder band at 1288 cm^{-1} corresponds to the vibration of OH attached to carbon, i.e., C–OH [22]. This band may not broaden by H-bonding as its stretching mode analogues. The band at 1725 cm^{-1} corresponds to the stretching vibrations of –C=O groups while the band at 1630 cm^{-1} due to O–C–O deformation and H-O-H bending modes (Fig. 3.I.A). Both –OH and –C–O bands are interesting to note as none were present in the spectrum obtained from vein graphite before the oxidation (i.e., sp^2 bonded carbon in graphite turns into sp^3 bonded carbon following the oxidation). The

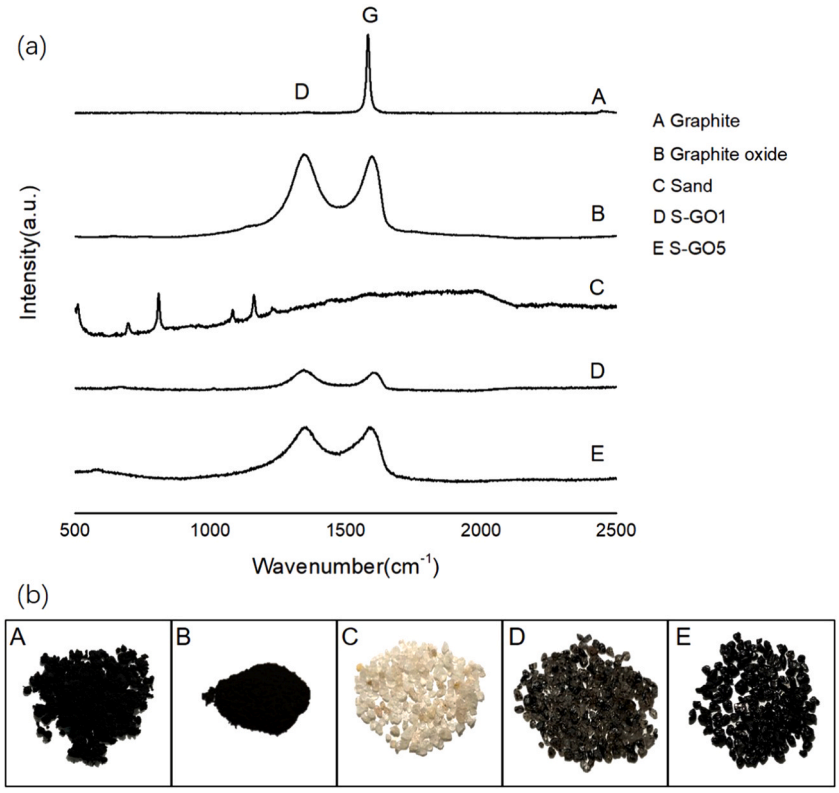

Fig. 2. (a) Raman spectrums of A: Graphite, B: Graphite oxide, C: Sand, D: S-GO1 and E: S-GO5. (b) Photo images, A: Graphite, B: Graphite oxide, C: Sand, D: S-GO1 and E: S-GO5.

presence of carbonyl groups (–C=O) on the basal plane of graphene oxide prepared using flake graphite has also been observed [20,22]. On some occasions, bands at 1630 cm^{-1}, 1408 cm^{-1}, and 590 cm^{-1} have been assigned to stretching vibrations and bending modes of GO structural –C=C–. The bands in the 1230–1030 cm^{-1} range can ascribe to ~ C-O single bond vibrations of ~ C–O and O=C–OH. The bands in the range of 860–750 cm^{-1} are due to C–O–C bending vibrations.

The bands at 1184 cm^{-1} and 1054 cm^{-1} corresponds to the epoxy (C–OH) and alkoxy (C–O) functional groups confirming the presence of GO. The IR spectrum of river sand shows broadband around 3500 cm^{-1} due to the stretching of H-bonded –-OH vibrations (Fig. 3.II). On its shoulder, narrow bands at 3650 cm^{-1} and 3720 cm^{-1} are due to symmetric and asymmetric stretching vibrations of the terminal –OH groups. Si–O–H bending mode vibrations are shown around 1080 cm^{-1} (Fig. 3.II).

The band at 850 cm^{-1} and 810 cm^{-1} are due to Si–O and Si–O–Si bending vibrations (Fig. 3.I.B). In single cycled GO coated sand, the band intensity at 3427 cm^{-1} is decreased and narrowed, which implies that some surface –OH groups are freed from the H-bonding network (Fig. 3.I.C). When GO coating on the sand was carried out in multiple cycles, the 3427 cm^{-1} band intensity decreased significantly indicating direct –OH in the sand and GO interactions (Fig. 3.I.D). The relative intensities of the terminal –OH bands of sand, i.e., 3650 and 3720 cm^{-1} retain to some extent. The intensity of the broadband at 1080 cm^{-1} due to –Si–O–H bending vibrations has decreased significantly upon interactions of GO with the surface sites of sand (Fig. 3.I.B and C). In the spectrum shown in Fig. 3.A–D, changing the peak patterns of 1230 and 590 cm^{-1} from distinct to broad nature can be ascribed to the resultant vibrational coupling from other modes such as ≡SiOH and ≡SiO-G-O ~ further confirming a clear interaction between sand and GO (Fig. 2.a.C–E). In sand, the discrete bands at 3650 and 3720 cm^{-1} are due to symmetric and asymmetric stretching vibrations of the terminal –OH groups and they suggest some ≡SiOH hydroxyl sites (silanols) abut from the surface (Fig. 3.II). Although ≡SiOH groups are ubiquitous on the sand surface, they are inert for $OH^- \rightleftharpoons F^-$ exchange reactions. The fluoride adsorption on bare sand is minimal (e.g., around 2% removal efficiency, Table 2). Therefore, the peaks at 3650 and 3720 cm^{-1} retain (Fig. 3.I.B). The network of H-bonded ≡SiOH sites limits the OH^- exchange with F^-. Upon GO coatings, the ≡SiOH groups seem free from the labyrinth of H-network due to perturbation of the local environment possibly creating a new site with enhanced fluoride adsorption (hereafter ≡GOH). Therefore, F^- can readily exchange with OH^- located on isolated ≡GOH sites of GO-coated sand, which is evident due to disappeared IR bands at 3650 and 3720 cm^{-1} on the S-GO5-F spectrum (Fig. 3.I.E).

3.3. Fluoride removal by reactivity enhanced sand

Conventionally, the sand filters are used to reduce water turbidity. We used S-GO5 and S-GO1 to examine the simultaneous removal of fluoride and turbidity in water. When 0.90 ± 0.01 g/L S-GO1 is used as an adsorbate, within an hour the turbidity of treated water has increased by about two-folds (Table 2). However, the adhered GO layers on S-GO5 do not peel off upon contact with the water. For example, when S-GO5 is equilibrated with the water for two months, the turbidity values never increased beyond 0.02 NTU.

The external surface charge of particulates in a suspension can be determined by IEP measurements. However, the net zero proton point of charge (NZPC) obtained by surface titrations varies in response to the net total (both external and internal) surface charge of the particles. The pH_{IEP} of GO is 2.10 [12], and the pH_{zpc} of quartz is 2.01[11]. Therefore, the charge of both surfaces is negative within the pH range typical of natural waters, viz. pH 6.0–8.5. Thus, interactions between sand & GO or GO & GO in water suspensions are repulsive. The S-GO1 surface is heterogeneous; however, it can regard as an array of isolated homogeneous domains for chemisorption of GO against electrostatic fields [12]. The honeycomb aromatic moieties of GO undergo π-π interactions among electron-rich and deficient regions, leading to layer stacking. Both H-bond donors and acceptors from epoxides, alcohols, ethers,

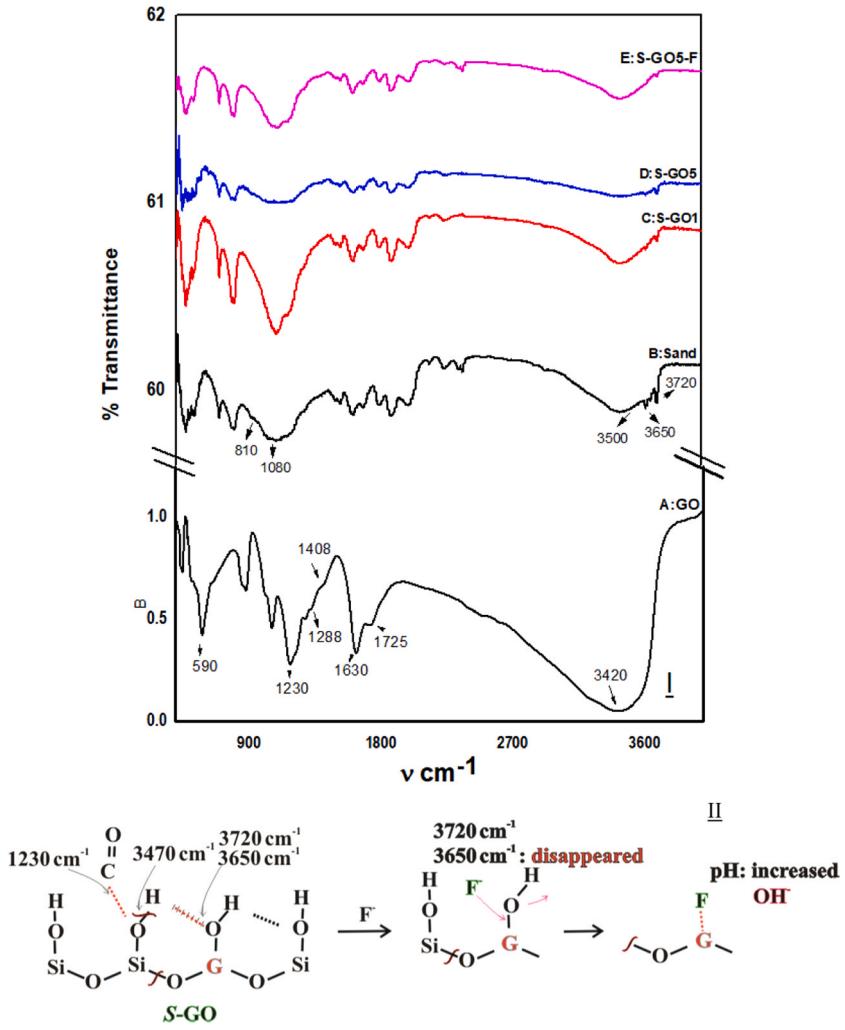

Fig. 3. I. Transmission Fourier transformed spectrums of GO, Sand, S-GO1, S-GO5 and fluoride adsorbed S-GO5 (S-GO5-F). II. Fluoride adsorption by S-GO composites.

Table 2
The chemical composition and $r_{F^-/OH}$ exchange ratio of treated water by S-GO1 and S-GO5. In % turbidity removal (+) indicates increased turbidity. The raw water pH 6.30 ± 0.02, turbidity, 0.08 ± 0.01 NTU, fluoride 2.00 mg/L.

Parameter	S-GO1	S-GO5	Sand
Solid ± 0.01 g/L	0.90	0.90	0.90
Initial F^- ± 0.01, mg/L	2.00	2.00	1.80
Adsorption capacity± 0.01, mg/g	0.89	1.56	0.40
Turbidity, NTU removal %	+ 75 ± 1	−87 ± 1	−50 ± 1
$r_{F-/OH-}$ exchange	0.80	0.98	not determined

carboxylic, and carboxylate oxygen-bearing moieties that are ubiquitous in GO can contribute to intra-molecular interactions with sand sites leading to enhanced stability of S-GO5 [8]. The pH_{nzpc} values of S-GO1 and S-GO5 are 4.2 and 6.3, respectively (Figure 6-S). At pH_{zpc}, $\sum_{all} \equiv GOH2^+ = \sum_{all} \equiv GO^-$ and the net surface charge is neutral, and a non-variable charge approach can be used to model fluoride adsorption. When compared to bare sand, both S-GO1 and S-GO5 show enhanced efficiency for fluoride removal in water. As discussed earlier (Table 2), when initial pH of the solution is around ~ 6.30, the S-GO1 removes 40% fluoride with simultaneous increase of the turbidity in the treated water. However, the S-GO5 removes around 70% fluoride while keeping water turbidity below 0.02 NTU due to stability of adhered GO layers on sand and attraction of other constituents that induce turbidity onto the substrate. The fluoride removal by S-GO1 is optimal at acidic solutions (typically pH ~ 3.22 ± 0.02, data not shown), whereas with the S-GO5 solutions with near-neutral pH (~6) are sufficient. When the solution pH ~ 6, neutral surface sites, denoted as ≡GOH play a role in fluoride adsorption. Additionally, in acidic pH, protonated ≡GOH sites ($\equiv GOH_2^+$) are also active in the removal of fluoride from the solution. Therefore, fluoride removal processes by S-GO composites can be given as:

$$\equiv GOH + H^+ + F^- = \equiv GF + H_2O \quad (1)$$

$$\equiv GOH + F^- = \equiv GF + OH^- \quad (2)$$

We noted that fluoride removal occurs via OH- exchange with a pH increase (Table 2 rF-/OH- data). Bare sand is not an efficient substrate for fluoride retention due to weak acidity of silanol groups [12]. However, upon activation of the sand with GO, its fluoride adsorption enhanced significantly. The release of hydroxyls by S-GO1 or S-GO5 upon fluoride sorption provides a qualitative measure for the nature of surface sites [16]. The r F-/ OH- value of 0.98 for S-GO5 implies that a stoichiometric exchange of fluoride per OH− via reaction (1). However, in S-GO1, r F-/ OH- 0.80 value indicates that both reactions are in operation for sorption of fluoride.

3.4. Modelling of fluoride adsorption by S-GO

The fluoride adsorption on S-GO1 and S-GO5 follows Freundlich and

Hill models, respectively (Fig. 4. A–B). We believe that an array of homogeneous domains leads to a heterogeneous surface. For S-GO1, the adsorption data complies with the Freundlich convention, which implies more than one such domain seems responsive for fluoride. In contrast, the shape of fluoride adsorption isotherm on S-GO5 is sigmoidal, as characterized by a small initial slope that increases with adsorptive concentration (Fig. 4. B). Hill quantified sigmoidal isotherms considering a reversible combination of a ligand with discrete binding sites at equilibrium as shown in

$$\Gamma_{F^-} = \frac{\Gamma_T K_H (F^-)^n}{1 + K_H (F^-)^n}$$

where Γ_{F^-} fluoride adsorption capacity (mg/kg), Γ_T maximum fluoride adsorption density, K_H Hill parameter, and n index for cooperative adsorption [23]. The non-integer value of n indicates weak cooperativity.

As in Fig. 4. B, we modelled the data according to the Hill model with n ~ 3.2, Γ_T ~ 3447 mg/kg, and K_H 3.32. It seems that fluoride ion retains cooperatively by about 3–4 discrete surface sites on S-GO5. The exact mechanism of fluoride retention by S-GO5 sites is controversial. However, it points out that fluoride traps within the network of sites often present in S-GO5 surfaces. As shown in Table 2, when S-GO5 is used no pH adjustments are required to yield optimal conditions for fluoride adsorption since the pH of most natural waters are around 6–7.

3.5. Kinetics of fluoride adsorption by S-GO1 and S-GO5

The exact adsorption mechanism of fluoride by GO-composites is not resolved to date. From a macroscopic viewpoint, the adsorption occurs through film diffusion, pore diffusion, and surface diffusion and adsorption on micropore surfaces; the relative contribution from each process requires further study. As shown in SEM micrographs, the S-GO particulates approximate to the morphological configuration of plate geometry with porous structures. When the mass transfer of fluoride ions from the bulk solution to the liquid – solution interface followed by the diffusion into the porous structure of S-GO composites, the fluoride

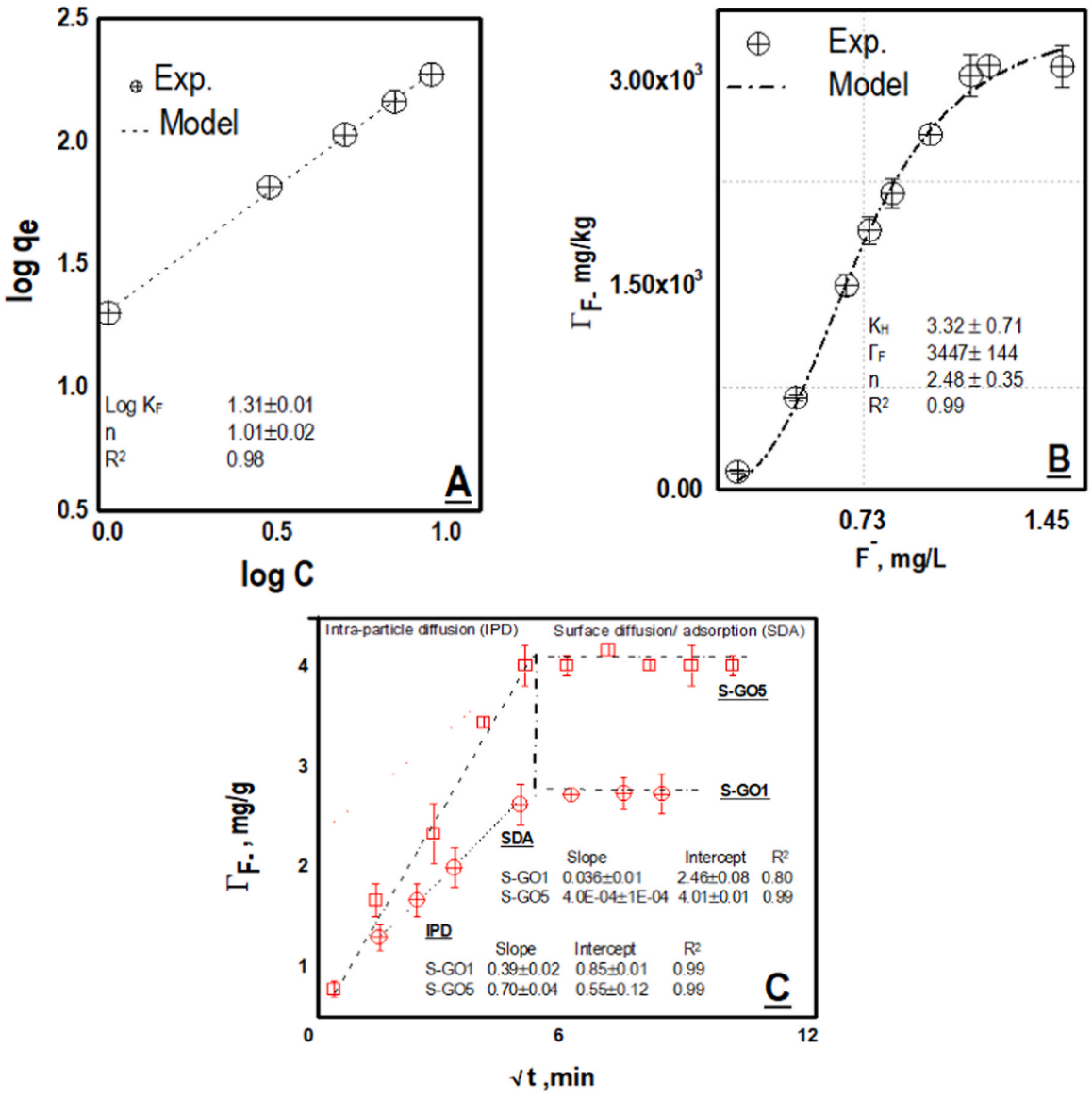

Fig. 4. (A-C) Fluoride adsorption on GO – sand composites. (A) S-GO1, modelled by Freundlich equation (B) S-GO5 Modelled with Hill Equation. (C) Kinetics plot of the variation fluoride adsorption as a function of $\sqrt{t}$. For sand, due to low fluoride adsorption density Γ_F vs $\sqrt{t}$ plots cannot be obtained. Initial fluoride 0.25–2.5 mg/L; solid content 0.5 g/L, T = 25 °C. Error bars show ± s.d. Symbols represent experimental data. Lines represent modelled data and legends show standard errors and goodness of fit of calculations.

adsorption can interpret with the intra-particle diffusion model as

$$q_t = k_t . \sqrt[n]{t} + C$$

where q_t is the amount of adsorbate at time t and k_t is the intraparticle diffusion rate constant, and the C is proportional to boundary layer thickness [24]. We assumed platy-like structures in the substrates, and also, Fickian mass transport approximates n ~ 0.5. Under these assumptions, the number of line segments in a given q_t vs $\sqrt{t}$ plot accounts for different mass transfer modes. Fig. 4 shows that the plots of fluoride sorption versus $\sqrt{t}$ for S-GO1 and S-GO5 represents multilinearity, which characterizes two steps, namely intra-particle diffusion and surface diffusion followed by adsorption [25]. The slope of the plot q versus $\sqrt{t}$ is defined as a rate parameter, characteristic of the rate of adsorption in the region where intra-particle diffusion is rate controlling. The extrapolation of straight lines gives Y-intercepts which are proportional to the boundary layer thickness. The larger the intercept, the more significant the contribution of the surface sorption in the rate-limiting step [26].

3.6. Fluoride removal efficiency by sand and S-GO composites

Fig. 5 and Table 2 show fluoride and turbidity removal efficiencies by S-GO1, S-GO5, and sand. In all cases, the feedwater has the following composition: pH 6.31, turbidity 0.08NTU and 2.00 mg/L fluoride. The sand removes less than 1% of fluoride and ~ 40% turbidity whereas S-GO5 removes 70% fluoride and 87% turbidity. S-GO1 removes only 40% fluoride. However, the turbidity of the treated water by S-GO1 has increased by 75% due to GO dissolution.

Further, the optimal solution pH for fluoride adsorption by S-GO1 is around 3.22 (data are not shown), and such extreme acidic conditions are rare in nature. In the presence of S-GO5, at near-neutral acidity conditions, over 70% of fluoride and turbidity can be removed, simultaneously. Therefore, S-GO5 shows excellent performance in the simultaneous removal of fluoride and turbidity from the water.

Following Li et al. [7], we calculated the S-GO5 mass required to treat 1000 L of 5 mg/L fluoride water to 1 mg/L as 1.0 kg. The efficiency of fluoride removal of Li et al. [7] method and ours are comparable, which shows five-told enhancement over aluminium derived activated carbon method [27]. However, for fluoride removal, Li et al. [7] used graphene, and we used sand coated GO (S-GO5) substrates. When using graphene, removal of fluoride-laden grapheme colloids from water poses additional issues. In S-GO5 the GO layers adhere to sand; hence particulate materials are no longer in the aqueous phase as colloids. Further, when compared to graphene, GO is environmentally benign [10]. However, further research needs under following directions; i. reusability of S-GO5, ii. feasibility of S-GO5 in the removal of other contaminants, and iii. incorporation of S-GO5 in conventional sand filter units.

4. Conclusions

Fluoride is a biologically active element and its primary source of human intake of fluoride in water. Therefore, the development of novel methods for its mitigation is timely due to its implications as a neurotoxicant. We fabricated stable, multi-layered sand-GO composites without using a binder. The sand surface progressively becomes positively charged with the increase of GO layering. Our graphite oxide coated sand has a core-shell configuration. We examined the suitability of surface-enhanced sand for the concurrent removal of fluoride and turbidity from the water. Optimal fluoride removal was around 70% at pH 6.31 ± 0.02 by multiply coated GO–sand (S-GO5). Fluoride adsorption occurs via intra-particle diffusion. The GO layers on S-GO1 water suspensions are not stable. The surface-enhanced sand by GO, e.g. S-GO5 can use for the simultaneous removal of fluoride and turbidity in water. Although the GO synthesis is costly, our S-GO5 can be mass produced. Further research is needed to evaluate reusability of S-GO5 in fluoride removal, and the potential of the substrate in treating other contaminants in water.

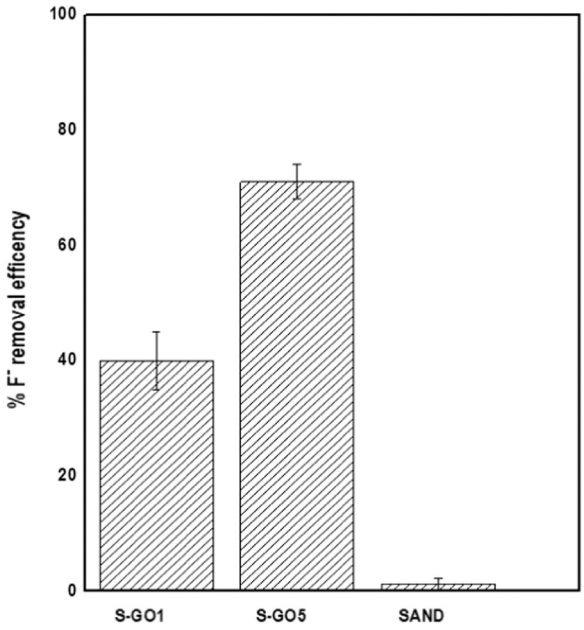

Fig. 5. Fluoride removal efficiencies by S-GO1, S-GO5 and sand. Initial fluoride concentration 2 mg/L in 0.01 M $NaNO_3$. Refer to Table 2 for details—error bars in ± s.d.

CRediT authorship contribution statement

A.R. Kumarasinghe: Conceptualization, Supervision, Writing - original draft. **W.P.R.T. Perera:** Validation. **J. Bandara:** Investigation. **P. Rukshagini**: Visualization. **Janitha A. Liyanage**: Project Administration. **R. Tennakone:** Investigation. **A. Bandara:** Methodology. **Xing CHEN:** Data curation, Formal analysis, Funding acquisition, Writing - review & editing. **Rohan Weerasooriya:** Funding acquisition, Resources, Writing - review & editing.

Declaration of Competing Interest

The authors declare that they have no known competing financial interests or personal relationships that could have appeared to influence the work reported in this paper.

Acknowledgements

Support for this project was received through the National Research Council of Sri Lanka under Target Driven Grant Scheme (NRC-TO-16–015). BET surface area measurements of the samples were carried out by Professor Tomonori Kawakami, Toyama Prefectural University, Japan. RW acknowledges the Program of Distinguished Professor in B & R Countries, PR China for Hefei University of Technology abidance (Grant No. DL20180052). Reviewers' comments greatly enhanced manuscript quality.

Declaration of Competing Interest

The authors declare that they have no known competing financial interests or personal relationships that could have appeared to influence the work reported in this paper. All authors declare no conflicts of interest and any financial benefits endowed from the work.

Appendix A. Supporting information

Supplementary data associated with this article can be found in the online version at doi:10.1016/j.jece.2020.104962.

References

[1] WHO, Inadequate or Excess Flouride: a major public health concern, 2019, pp. 1–5.
[2] P. Grandjean, Developmental fluoride neurotoxicity: an updated review, Environ. Health. A Glob. Access Sci. Source 18 (2019) 1–17, https://doi.org/10.1186/s12940-019-0551-x.
[3] R. Liteplo, R. Gomes, WHO, environmental health criteria 227, Fluoride, World Helth Organ., Geneva 290 (2002).
[4] S. Jagtap, M.K. Yenkie, N. Labhsetwar, S. Rayalu, Fluoride in drinking water and defluoridation of water, Chem. Rev. 112 (2012) 2454–2466, https://doi.org/10.1021/cr2002855.
[5] G.K. Sarma, M.H. Rashid, Synthesis of Mg/Al layered double hydroxides for adsorptive removal of fluoride from water: a mechanistic and kinetic study, J. Chem. Eng. Data 63 (2018) 2957–2965, https://doi.org/10.1021/acs.jced.8b00242.
[6] L. Kuang, Y. Liu, D. Fu, Y. Zhao, FeOOH-graphene oxide nanocomposites for fluoride removal from water: Acetate mediated nano FeOOH growth and adsorption mechanism, J. Colloid Interface Sci. 490 (2017) 259–269, https://doi.org/10.1016/j.jcis.2016.11.071.
[7] Y. Li, P. Zhang, Q. Du, X. Peng, T. Liu, Z. Wang, Y. Xia, W. Zhang, K. Wang, H. Zhu, D. Wu, Adsorption of fluoride from aqueous solution by graphene, J. Colloid Interface Sci. 363 (2011) 348–354, https://doi.org/10.1016/j.jcis.2011.07.032.
[8] V. Georgakilas, J.N. Tiwari, K.C. Kemp, J.A. Perman, A.B. Bourlinos, K.S. Kim, R. Zboril, Noncovalent functionalization of graphene and graphene oxide for energy materials, Biosens. Catal. Biomed. Appl. Chem. Rev. 116 (2016) 5464–5519, https://doi.org/10.1021/acs.chemrev.5b00620.
[9] Y. Chang, S. Yang, J. Liu, E. Dong, Y. Wang, A. Cao, Y. Liu, H. Wang, In vitro toxicity evaluation of graphene oxide on A549 cells, Toxicol. Lett. 200 (2011) 201–210, https://doi.org/10.1016/j.toxlet.2010.11.016.
[10] C. Liao, Y. Li, S.C. Tjong, Graphene nanomaterials: synthesis, biocompatibility, and cytotoxicity, Int. J. Mol. Sci. 19 (2018) 1–34, https://doi.org/10.3390/ijms19113564.
[11] X. Fan, D.J. Parker, M.D. Smith, Adsorption kinetics of fluoride on low cost materials, Water Res. 37 (2003) 4929–4937, https://doi.org/10.1016/j.watres.2003.08.014.
[12] N.P. Sotirelis, C.V. Chrysikopoulos, Interaction between graphene oxide nanoparticles and quartz sand, Environ. Sci. Technol. 49 (2015) 13413–13421, https://doi.org/10.1021/acs.est.5b03496.
[13] P.W. Sutter, J.I. Flege, E.A. Sutter, Epitaxial graphene on ruthenium, Nat. Mater. 7 (2008) 406–411, https://doi.org/10.1038/nmat2166.
[14] W. Gao, M. Majumder, L.B. Alemany, T.N. Narayanan, M.A. Ibarra, B.K. Pradhan, P.M. Ajayan, Engineered graphite oxide materials for application in water purification, ACS Appl. Mater. Interfaces 3 (2011) 1821–1826, https://doi.org/10.1021/am200300u.
[15] J. Chen, B. Yao, C. Li, G. Shi, An improved hummers method for eco-friendly synthesis of graphene oxide, Carbon 64 (2013) 225–229, https://doi.org/10.1016/j.carbon.2013.07.055.
[16] D.A. Dzombak, F.M.M. Morel, Surface Complexation Modeling: Hydrous Ferric Oxide, Wiley, New York, 1990.
[17] I.R.M. Kottegoda, X. Gao, L.D.C. Nayanajith, C.H. Manorathne, J. Wang, J.Z. Wang, H.K. Liu, Y. Gofer, Comparison of few-layer graphene prepared from natural graphite through fast synthesis approach, J. Mater. Sci. Technol. 31 (2015) 907–912, https://doi.org/10.1016/j.jmst.2015.07.014.
[18] R.C. Rollings, A.T. Kuan, J.A. Golovchenko, Ion selectivity of graphene nanopores, Nature, Communications 7 (2016), https://doi.org/10.1038/ncomms11408.
[19] G.L. Wen, W. Zhao, X. Chen, J.Q. Liu, Y. Wang, Y. Zhang, Z.J. Huang, Y.C. Wu, N-doped reduced graphene oxide /MnO2 nanocomposite for electrochemical detection of Hg2+ by square wave stripping voltammetry, Electrochim. Acta 291 (2018) 95–102, https://doi.org/10.1016/j.electacta.2018.08.121.
[20] I.K. Moon, J. Lee, R.S. Ruoff, H. Lee, Reduced graphene oxide by chemical graphitization, Nat. Commun. 1 (2010), 73, https://doi.org/10.1038/ncomms1067.
[21] S.A. Bradford, S. Torkzaban, Colloid adhesive parameters for chemically heterogeneous porous media, Langmuir 28 (2012) 13643–13651, https://doi.org/10.1021/la3029929.
[22] M.K. Rabchinskii, A.T. Dideikin, D.A. Kirilenko, M.V. Baidakova, V.V. Shnitov, F. Roth, S.V. Konyakhin, N.A. Besedina, S.I. Pavlov, R.A. Kuricyn, N.M. Lebedeva, P.N. Brunkov, A.Y. Vul, Facile reduction of graphene oxide suspensions and films using glass wafers, Sci. Rep. 8 (2018) 1–11, https://doi.org/10.1038/s41598-018-32488-x.
[23] H. Swenson, N.P. Stadie, Langmuir's theory of adsorption: a centennial review, Langmuir 35 (2019) 5406–5426, https://doi.org/10.1021/acs.langmuir.9b00154.
[24] S. Nethaji, A. Sivasamy, A.B. Mandal, Adsorption isotherms, kinetics and mechanism for the adsorption of cationic and anionic dyes onto carbonaceous particles prepared from Juglans regia shell biomass, Int. J. Environ. Sci. Technol. 10 (2013) 231–242, https://doi.org/10.1007/s13762-012-0112-0.
[25] V. Vadivelan, K. Vasanth Kumar, Equilibrium, kinetics, mechanism, and process design for the sorption of methylene blue onto rice husk, J. Colloid Interface Sci. 286 (2005) 90–100, https://doi.org/10.1016/j.jcis.2005.01.007.
[26] V. Fierro, V. Torné-Fernández, D. Montané, A. Celzard, Adsorption of phenol onto activated carbons having different textural and surface properties, Microporous Mesoporous Mater. 111 (2008) 276–284, https://doi.org/10.1016/j.micromeso.2007.08.002.
[27] R. Leyva Ramos, J. Ovalle-Turrubiartes, M.A. Sanchez-Castillo, Adsorption of fluoride from aqueous solution on aluminum-impregnated carbon, Carbon 37 (1999) 609–617, https://doi.org/10.1016/S0008-6223(98)00231-0.